This manuscript is a non-peer reviewed preprint submitted to EarthArXiv.
It has been submitted to Geophysical Journal International (GJI) for peer review.

submitted to *Geophys. J. Int.*

Unlocking the potential of single stations to replace seismic arrays

Jana Klinge[1], Sven Schippkus[1], and Céline Hadziioannou[1]

[1] *Institute of Geophysics, Center for Earth System Research and Sustainability (CEN), University of Hamburg, Hamburg, Germany*

SUMMARY

We introduce Virtual Seismic Arrays, which predict full array recordings from a single reference station, eliminating the need for continuous deployment of all stations. This innovation can reduce costs and logistical challenges while maintaining multi-station functionality. We implement a Virtual Seismic Array using a deep learning encoder-decoder approach to predict transfer properties between stations. Training on recordings from the Gräfenberg array in the secondary microseism frequency band allows us to retrieve models capturing transfer characteristics between stations. These models form the Virtual Seismic Array. To evaluate performance, we beamform original and predicted waveforms to detect dominant secondary microseism sources. We assess three scenarios: one aligning with the training dataset, another with two regimes in training but testing on one, and a third where training data does not align with the testing regime. Our results show strong agreement between predicted and original beamforming results, demonstrating the potential of Virtual Seismic Arrays.

Key words: Machine learning; Time-series analysis; Seismic noise; Seismic array; Wave propagation

1 INTRODUCTION

Seismic arrays are an essential approach to collect and analyze seismic data, improving the understanding of geophysical processes like seismic source localization and determination of large- and fine-scale structures of the Earth's interior (Gibbons & Ringdal 2006; Rost & Thomas 2009; Schweitzer et al. 2012). By increasing the capability to detect seismic events, seismic arrays significantly improve seismic monitoring and allow for insights into wave propagation phenomena. An essential processing technique enabling this is beamforming, which allows directional signal detection by combining multiple sensor inputs, thereby improving signal-to-noise ratio and allowing seismic arrays to operate as wave number filters (Capon et al. 1967; Rost & Thomas 2002; Wang et al. 2020). Array beamforming is also widely applied in other fields, such as ultrasound and astronomy, where it improves image resolution and diagnostic precision (Lu et al. 1994; Holfort et al. 2009; Luijten et al. 2020), as well as the sensitivity of observations (van der Veen et al. 2004; Warnick et al. 2016).

This research aims to advance seismic observation techniques by introducing the concept of Virtual Seismic Arrays, which could help vastly decrease costs and improve monitoring in environments with limited resources or insufficient seismic infrastructure. A Virtual Array is able to acquire seismic data from previously instrumented areas even after the physical sensors have been removed. The concept includes the prediction of array recordings based on data from a single reference station, which was originally part of the array, thereby eliminating the need for continuous deployment of all array stations. While multiple stations often provide advantages in event location and signal characterization (Gibbons & Ringdal 2006; Rost & Thomas 2009), they can be challenging to deploy, require regular maintenance, and are associated to high operating costs. Our new approach uses deep learning to achieve capabilities similar to those of seismic arrays with just a single station. By learning signal propagation characteristics between a reference station and all stations within a seismic array, our method maintains the ability to monitor seismic activity effectively, while significantly reducing the physical infrastructure required. We note that the term "virtual seismic array" has been used before in a different context (Alhukail 2012), where it refers to an approach for enhancing the response of an existing seismic array. In contrast, our approach aims to allow the continued operation of seismic arrays after most stations have been removed from the field.

Encoder-decoder networks, a type of neural network, have been widely applied in seismology to learn complex patterns from seismic data enabling earthquake event classification (Li et al. 2022), fault detection (Li et al. 2019) or seismic inversion (Gelboim et al. 2023). Klinge et al. (2025) employed encoder-decoder networks that represent the transfer function between two seismic stations by learning the underlying signal transformations. Within a supervised framework, the network is trained with time series data from a fixed seismic reference station to successfully predict measurements of different neighboring stations (Klinge et al. 2025).

We investigate the applicability of encoder-decoder networks to realize Virtual Seismic Arrays. As a proof-of-concept, we train a Gräfenberg Virtual Seismic Array in the secondary microseism frequency band (0.1 to 0.3 Hz), where wind-driven ocean waves interact with the solid Earth, resulting in continuous seismic noise detectable on land (Longuet-Higgins & Jeffreys 1950; Hasselmann 1963; Ardhuin et al. 2019). By using beamforming techniques, we analyze the noise signals recorded in the given frequency band to identify and differentiate the dominant wave type regimes present in the seismic noise field. In the following, we describe the data used, the network architecture and compare beamforming results on original and predicted recordings.

2 DATA AND METHODS

2.1 Seismic data and beamforming

We train the neural networks with data from the Gräfenberg seismic array (GRF), which consists of 13 seismic broadband stations (Harjes et al. 1977). The array is located in the Franconian Jura in central Bavaria, Germany, extending approximately 100 kilometers north-south and 40 kilometers east-west (Fig. 1a). We select two time frames for analysis, each consisting of two days of data from all array stations, with one frame corresponding to summer (July 2013) and the other to winter (November 2013), chosen to avoid earthquakes. To prepare the data for the neural network training, we remove the instrument response, detrend, and demean. Seismograms are filtered in the secondary microseism frequency band using a Butterworth bandpass filter from 0.1 Hz to 0.25 Hz. Finally, we resample the data to 20 Hz.

Beamforming enables the extraction of propagation characteristics of seismic waves by analyzing the waveforms recorded across the array (Rost & Thomas 2002; Ruigrok et al. 2017). We use cross-correlation beamforming, which applies the delay-and-sum approach (Rost & Thomas 2002) to correlation functions in order to estimate the dominant direction of arrival (backazimuth) and slowness. This method assumes plane waves propagating across the array and is closely connected to Bartlett beamforming (Baggeroer et al. 1988). Both, backazimuth and slowness, not only provide important insights into the seismic waves being analyzed, but, in this study, are the quantities we use to validate the quality of the Virtual Seismic Array.

[ht]

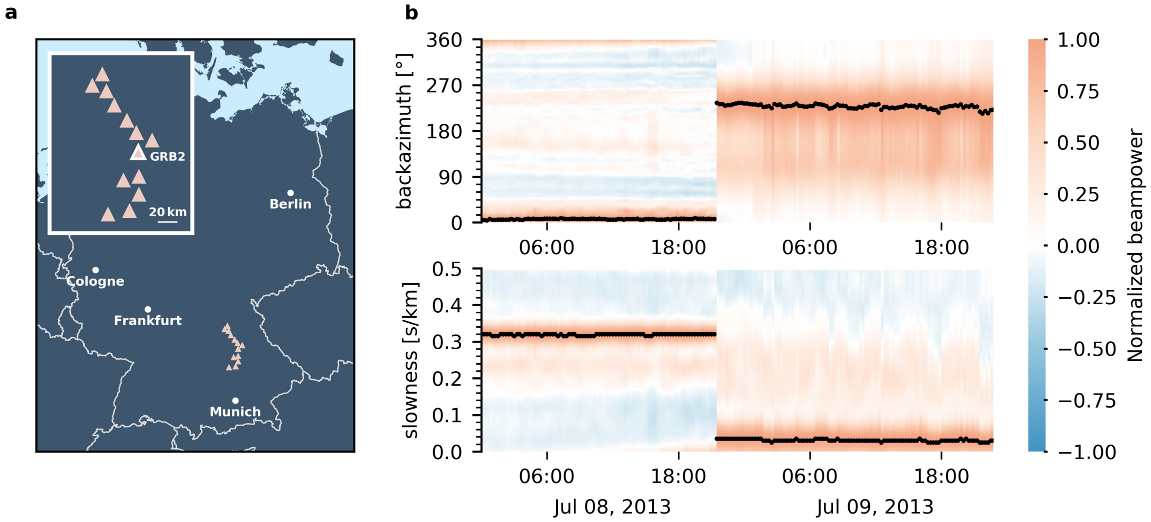

Figure 1. Gräfenberg array beamforming. **a** Map of Germany showing the location of the Gräfenberg (GRF) array, with seismic stations indicated by orange triangles. The reference station GRB2 is indicated with a white frame. An inset in the top-left corner provides a zoomed-in view of the station arrangement within the array. **b** Beamforming results for the selected two-day time period during summer. Colors indicate the normalized beampower in each slice along the best-fitting backazimuth and slowness dimensions. The best-fitting backazimuth and slowness are indicated with a black dot.

We apply beamforming to the original GRF recordings using 1-hour windows with 75% overlap. It is important to note that station GRB2 serves as the reference station and is therefore excluded in the beamforming. Figure 1b shows backazimuth and slowness for the selected two-day summer period. Background colors are slices through the slowness domain normalized by beampower, highlighting the best-fitting backazimuth and slowness with a black dot. During the first 22 hours, we observe waves from the north, with a single dominant backazimuth of 7°, measured clockwise from North, and slowness of 0.32 s/km (Fig. 1b). We call this the surface wave-dominated regime due to the presence of Rayleigh waves in this frequency range (Juretzek & Hadziioannou 2016). We further observe a stark transition to waves arriving from the southwest, with backazimuth and slowness values of 235° and 0.03 s/km, respectively, indicating the transition to a body wave-dominated regime (Landès et al. 2010; Pedersen & Colombi 2018; Lu et al. 2022; Zhang et al. 2023). These are the regimes we refer back to later in the text.

2.2 Waveform prediction

To obtain the models that predict seismic waveforms and together constitute the Virtual Seismic Array, we build on the approach introduced by Klinge et al. (2025). By learning the transfer functions between a reference station and all other stations within a given seismic array, we obtain unique models that capture the transfer characteristics for each station pair individually. This allows modeling data at each station even if they are no longer in operation, provided that the reference station is still installed and running. We select GRB2 as the reference station because it is located near the center of the array (Fig. 2a).

Klinge et al. (2025) used an encoder-decoder network to learn the transfer properties between two seismic stations. We use the same network architecture with minor changes to account for the different sampling frequency and frequency band. The approach involves feeding input data from a seismic reference station to the network, with the aim of learning the transfer to target data from a neighboring seismic station. As a result, the network generates predictions that ideally approximate the waveforms of the target data. We demonstrate that this methodology is applicable not only to the original study's data but also to the GRF array. While the original study involved an array with interstation distances of hundreds of meters (about seven wavelengths) and varying sources, like oil pumps, at frequencies below 10 Hz, we now apply the methodology to the GRF array with tens of kilometers between stations and in the frequency range of 0.1–0.25 Hz. Figure 2b illustrates example results from training the network with GRF array data, comparing target data and predictions for each station alongside the corresponding correlation coefficient (CC) for quality assessment. While amplitude predictions show variability, resulting in over- or underestimation, phase information is consistently well predicted, which is essential for effective beamforming applications. Although our average CC values are lower than those reported by Klinge et al. (2025), the maximum CC value we achieve is comparable to the results, highlights that the algorithm has the potential to capture key aspects of wave propagation in the GRF data as well.

Based on this methodology we perform the network training for every station combination with the reference station GRB2. Before training, the data are scaled with a combination of standard scaling and normalization. We allocate 80% of the data to the training set and 20% to the testing set. The testing set consists of data that the model has not seen during training (e.g. target data in Fig. 2b), allowing us to evaluate how well the algorithm generalizes to new data. The performance of the models on the testing data of each station represents the Virtual Seismic Array, enabling the prediction of seismic data across the array even if stations encounter failures or downtimes.

[ht!]

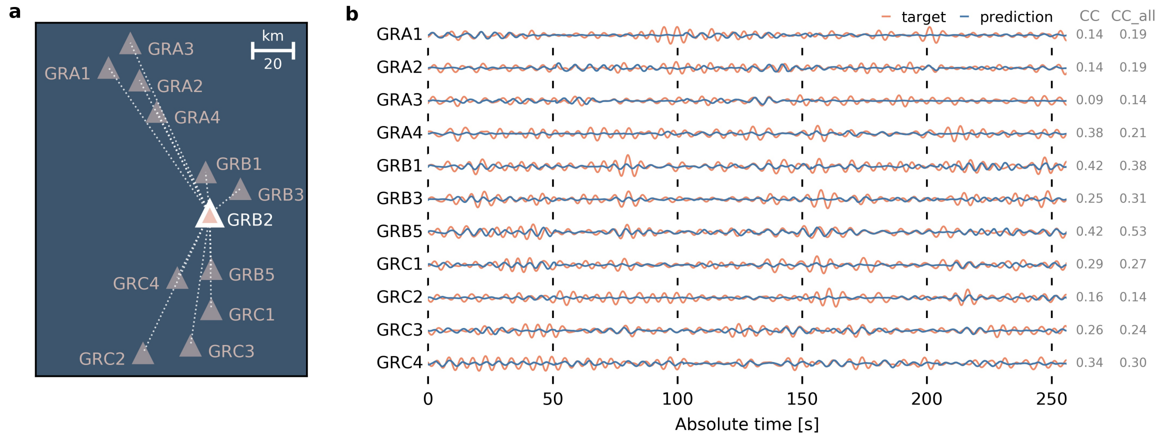

Figure 2. The Virtual Seismic Array. **a** The arrangement of stations within the Virtual GRF Array, highlighting the reference station GRB2 with a bold white outline, while the virtual stations are displayed in faded orange. Dashed lines illustrate the connections from the reference station to each of the array stations, forming station pairs for model training. **b** A selection of example data, featuring the target time series, i.e., the original recording, for each station (orange line) and the corresponding model predictions (blue line). The normalized correlation coefficient is provided on the right side for the example trace depicted (CC) as well as for the entire target data (CC_all), indicating the degree of similarity between the two time series.

3 PERFORMANCE OF THE VIRTUAL SEISMIC ARRAY

We evaluate the performance of the Virtual Seismic Array across three different scenarios of increasing complexity. First, we analyze a single dominant noise regime, characterized by surface waves only for both the training and testing data. Next, we evaluate its adaptability to a changing regime by training the models with data that transition from surface wave-dominance to body wave-dominance (Fig. 1b). Finally, we assess the performance for an unseen regime, where surface waves dominate in training but body waves dominate in testing. In the following, ”real array” refers to the original data, where all stations are still active. Our predictions constitute the Virtual Array.

3.1 A single dominant regime

For a single dominant regime (Fig. 3) we find that backazimuth and slowness detected by the real array in the test data (Fig. 3c,d) closely match those in the training set (Fig. 3a,b). The Virtual Array detects the same dominant backazimuth and slowness (Fig. 3e,f). Both the real and Virtual Array find surface waves incoming from North. The predicted slowness closely matches the original measurements, showing precise and focused detections.

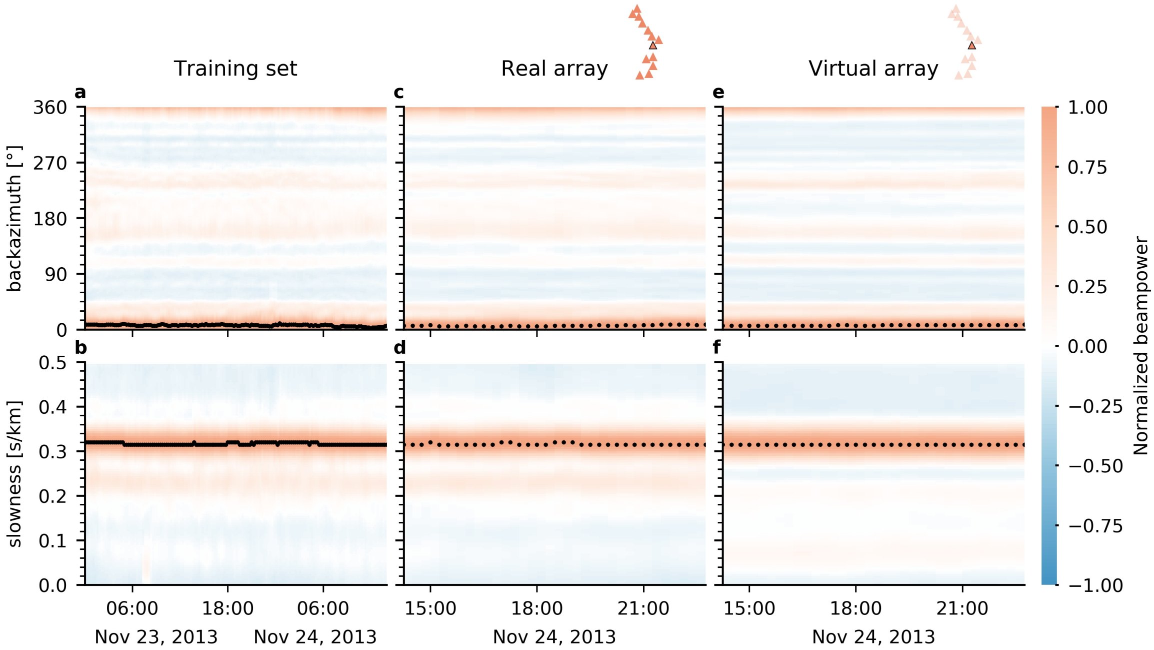

[ht!]

Figure 3. Beamforming results for the single dominant regime, with backazimuth in the top row and slowness in the bottom row. Panels **a** and **b** show results for the training set, which includes the first 80% of the two-day winter data dominated by surface waves. Panels **c** and **d** highlight results from the real array as ground truth, representing the last 20% of the two-day winter data, while panels **e** and **f** illustrate findings for the Virtual Array. Each plot includes background slices through the slowness domain, where blue indicate negative correlation and red indicate positive correlation. Black dots mark the maximum beampower, representing best-fitting waves.

The strong correspondence between the performance of the real array and Virtual Array demonstrates the proposed method effectively learns and predicts relevant seismic features in the data, despite low correlation coefficients. This highlights the algorithm's ability to capture the transfer characteristics between each station pair during training and to apply this knowledge to unseen data, showing its robustness with less than two days of training data. Our findings indicate the algorithm performs particularly well when the dominant noise regime is stable and aligns with the training dataset. Given that the model was trained on and applied to a single type of wave regime, we anticipated good performance. The question remains whether the Virtual Array can achieve similar predictive accuracy in more complex scenarios.

3.2 A changing regime

We investigate a more complex scenario, where the dominant regime changes (Fig. 4). Here, the training set contains a transition from surface to body wave-dominated regime, indicated by backazimuths and slownesses. We show the training set twice (Fig. 4a,b & g,h) to visually emphasize the application to two different testing datasets. First, we apply the models to body wave-dominated test data from the summer period post training set (Fig. 4c-f). Second, we evaluate the performance of the models on surface wave-dominated test data from the winter period (Fig. 4i-l). This cross-application helps to investigate the algorithm's ability to generalize and precisely capture seismic wave behavior under varying conditions.

In the first case, beamforming the Virtual Array reveals body waves arriving from southwest (Fig. 4e,f), similar to the direction observed by the real array (Fig. 4c,d). While the Virtual Array shows a very stable distribution of beampower values with time (Fig. 4e), the real array results deviate slightly from the average (Fig. 4c). In this example, the real array (Fig. 4c,d) detects less well-focused beampowers compared to those in the single dominant regime (Fig. 3), likely due to the presence of more complex wavefields and lower resolution at low slownesses. In contrast, the Virtual Array (Fig. 4e,f) finds remarkably sharp detections.

In the second case, beamforming the Virtual Array (Fig. 4k,l) detects predominantly surface waves coming from the north, which aligns well with detections by the real array (Fig. 4i,j). The observed values are in line with the surface wave-dominated regime seen in the first 22 hours of the training set (Fig. 4g,h), although body waves dominate the second part of the training set. For both the real array and Virtual Array, the beampowers are sharply focused around the maxima.

These two scenarios show that the algorithm is able to predict the wavefield from a single-station recording as long as the wavefield regime, i.e., dominant wave type and direction, has been part of the training. This highlights the algorithm's ability to generalize to more complex training sets compared to the single dominant regime while effectively differentiating between two distinct regimes. The sharper beampower focus for body waves detected by the Virtual Array compared to the real array supports this further (Fig. 4a-f). Although the algorithm was trained on both body and surface wave-dominated regimes, in the first case, the real array is dominated by body waves only, while in the second case, it is dominated by surface waves only. The models predict a simpler dominant wavefield compared to the original training set, resulting in sharper predictions and enhanced predictive accuracy.

Note that each time window is predicted independently from its neighboring time windows so that the prediction for a beamforming window is not affected by previous or later predictions. The algorithm furthermore successfully predicts the correct wavefield across seasons, with models trained on data

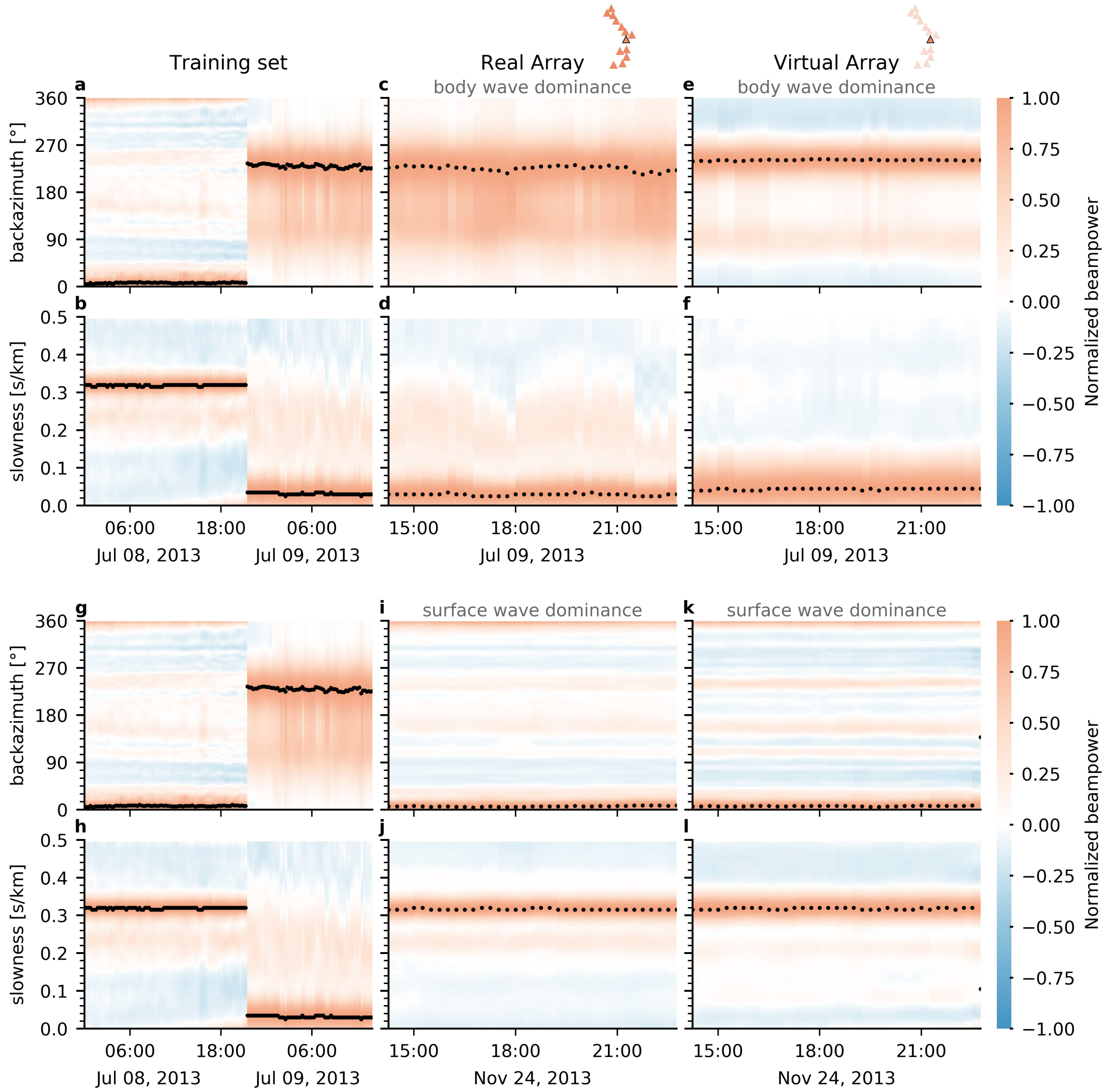

Figure 4. Beamforming results for the changing regime. The training set consists of the first 80% of the two-day summer data dominated by surface and body waves (**a**, **b**, **g**, and **h**). Panels **c** and **d**: Results from the real array, displaying the last 20% of the summer data, which is body wave-dominated, while panels **i** and **j** feature data from the real array during winter with a surface wave-dominance. Outcomes for the respective Virtual Arrays are illustrated in panels **e**, **f** and **k**, **l** . For further description of the plot see caption of Figure 3.

from summer being applied to winter data. This demonstrates its ability to generalize across seasonal variations of noise.

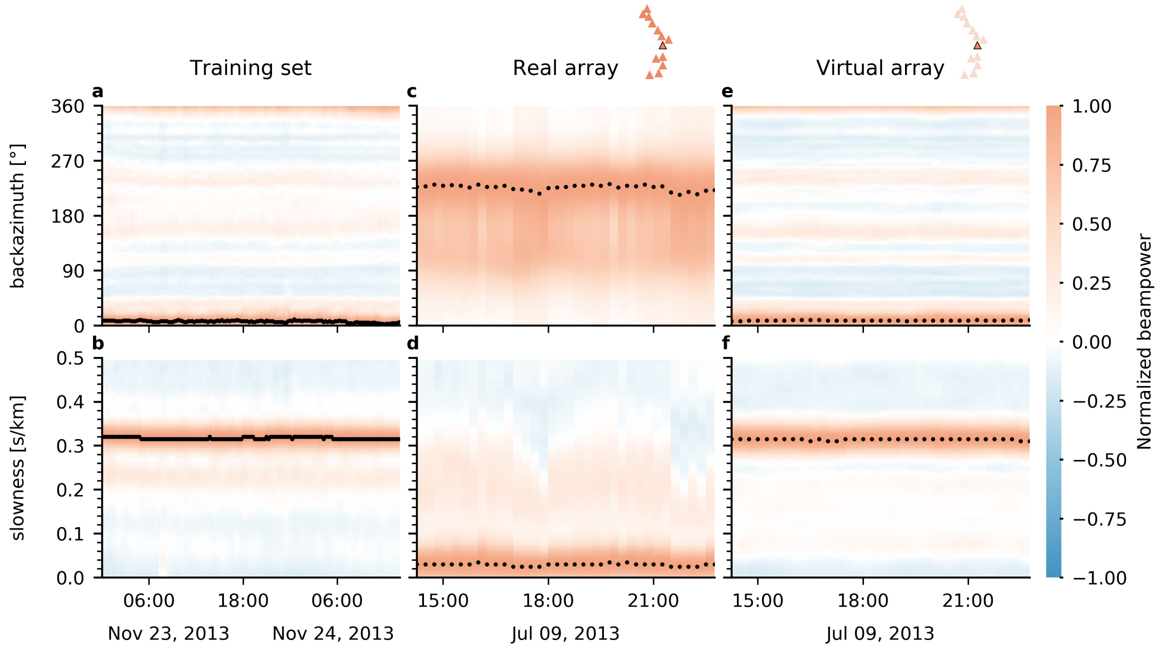

Figure 5. Beamforming results for the unseen regime. Panels **a** and **b** show the training set consisting of the first 80% of the two-day winter data dominated by surface waves. In panels **c** and **d**, results from the real array are displayed, showing body wave-dominance during the summer period. The outcomes of the Virtual Array are illustrated in panels **e** and **f**. For further description of the plot see caption of Figure 3.

3.3 An unseen regime

We demonstrate the main limitations of this approach by evaluating the algorithm's performance when encountering an unseen wavefield regime. The training set consists mainly of surface waves arriving from the north (Fig. 5a,b). Meanwhile, the original recordings of the real array are dominated by body waves arriving from the southwest (Fig. 5c,d). The Virtual Array is unable to predict the wavefield seen by the real array (Fig. 5e,f). Instead, it predicts surface waves arriving from north, the only wavefield regime it was trained on. This misalignment indicates a lack of generalization, suggesting that the models cannot adapt to the conditions present in the real array.

The algorithm fails to make accurate predictions when faced with a wavefield regime that was not included in the training set, as is the case for the unseen regime. The training set predominantly includes surface waves, which do not match the characteristics present in the real array, which are predominantly body waves. These limited generalization capabilities highlight that the algorithms effectiveness in making accurate predictions relies on the characteristics it encounters during the training process. However, when similar characteristics are present in the training set, as demonstrated in the single and the changing regime, the beamforming results for the Virtual Array are of high accuracy

(Figs. 3,4). Furthermore, it is likely that the models can only predict cases that have been encountered frequently during the training process. For earthquakes, which are intentionally excluded in the selected data, accurate predictions would therefore require training on datasets that include many examples. This limitation of encoder-decoder models for earthquake recordings has been reported before (Mousavi et al. 2020; Yin et al. 2022; Zlydenko et al. 2023). For our study, this underscores the importance of having a diverse training set that covers various regimes to enhance the algorithm's ability to generalize and make accurate predictions on different data characteristics. Therefore, we chose ocean microseism noise for this first demonstration of Virtual Seismic Arrays, as it is particularly well-suited due to its stability over days and weeks (Ardhuin et al. 2019).

4 APPLICATIONS AND OUTLOOK

Our findings demonstrate that Virtual Seismic Arrays can work and deliver promising wavefield predictions. As a result, several potential applications emerge, especially in remote areas where seismic array deployment can be challenging. By training models capable of predicting waveforms even without physical sensors, we can reduce the need for continuously deploying all array stations. For example, data from previous short-term deployments could be used as the training set, enabling ongoing predictions in the area of interest and maintaining data coverage without physical deployment of the full array. New deployments can be planned that involve using a minimal number of stations initially and repositioning those stations step by step to achieve full regional coverage over time while reducing the amount of resources needed. On an operational level, this approach also allows to compensate for temporary outages of individual stations. However, to fully realize Virtual Seismic Arrays in production, further steps are necessary. These include evaluating the performance in more complex datasets, such as those with frequent transitions between different wave type regimes and including transient sources such as earthquakes. It is important to integrate our findings with other approaches to enhance the adaptability of this method in different contexts. Additionally, understanding the most suitable conditions for implementing Virtual Seismic Arrays should be accompanied by detailed parameter studies. It is particularly important to understand, why certain station combinations are more effective than others and to assess how data quality and specific hyperparameters influence the model training, which we aim to pursue in the future.

5 CONCLUSION

In this study, we evaluate the applicability of encoder-decoder networks to implement Virtual Seismic Arrays, which predict data for an entire array using a single reference station. As a proof-of-concept, we train a Gräfenberg Virtual Seismic Array in the secondary microseism frequency band. By leveraging data from a single reference station to predict array recordings for all other stations within the array, we train models that successfully capture the wavefield propagation across the stations. Beamforming the resulting predicted waveforms reveals good agreement between the real and Virtual Array when the dominant wave regime encountered is included in the training set. This highlights the effectiveness of our approach in capturing underlying wave dynamics and the potential for future applications of Virtual Seismic Arrays. We propose to expand the application of this framework to diverse regions and seismic conditions, unlocking its potential to significantly enhance approaches for measuring and analyzing seismic data, particularly in challenging, remote areas. Temporary array deployments, for instance, can enable long-term "virtual operation" that allows seismic monitoring to continue when the physical array is unavailable. We test the most extreme version of a Virtual Array, where all but one station are removed and show that this approach can effectively compensate temporarily unavailable stations. This cost-effective advancement offers a promising approach for improving data availability and has the potential to substantially improve the reliability and efficiency of our global seismic monitoring capabilities.

DATA AVAILABILITY

We use publicly available seismograms provided by the German Regional Seismic Network (GR) operators (Federal Institute for Geosciences and Natural Resources 1976), accessed via the ORFEUS European Integrated Data Center (EIDA). We use accessible colors (Crameri 2023; Tol 2025).

Acknowledgements

The authors thank the BGR for seismic data access. This work is financially supported by the Federal Ministry of Education and Research (BMBF) project "3G-GWD" with references 05A20GU5 and 05A23GU5 and partially funded by the European Union's Horizon 2020 research and innovation programme under the Marie Skłodowska-Curie grant agreement No. 955515 (SPIN ITN - https://spin-itn.eu).

REFERENCES

Alhukail, I., 2012. *The Concept of Virtual Arrays in Seismic Data Acquisition*, Ph.D. thesis, Texas A&M University.

Ardhuin, F., Gualtieri, L., & Stutzmann, E., 2019. Physics of Ambient Noise Generation by Ocean Waves, pp. 69–108.

Baggeroer, A. B., Kuperman, W. A., & Schmidt, H., 1988. Matched field processing: Source localization in correlated noise as an optimum parameter estimation problem, *The Journal of the Acoustical Society of America*, **83**(2), 571–587.

Capon, J., Greenfield, R., & Kolker, R., 1967. Multidimensional maximum-likelihood processing of a large aperture seismic array, *Proceedings of the IEEE*, **55**(2), 192–211.

Crameri, F., 2023. Scientific colour maps.

Federal Institute for Geosciences and Natural Resources, 1976. German Regional Seismic Network (GRSN).

Gelboim, M., Adler, A., Sun, Y., & Araya-Polo, M., 2023. Encoder–Decoder Architecture for 3D Seismic Inversion, *Sensors*, **23**(1).

Gibbons, S. J. & Ringdal, F., 2006. The detection of low magnitude seismic events using array-based waveform correlation, *Geophysical Journal International*, **165**(1), 149–166.

Harjes, H.-P., Seidl, D., & others, 1977. Digital recording and analysis of broad-band seismic data at the Gräfenberg (GRF) array, *Journal of Geophysics*, **44**(1), 511–523.

Hasselmann, K., 1963. A statistical analysis of the generation of microseisms, *Reviews of Geophysics*, **1**(2), 177–210.

Holfort, I. K., Gran, F., & Jensen, J. A., 2009. Broadband minimum variance beamforming for ultrasound imaging, *IEEE Transactions on Ultrasonics, Ferroelectrics, and Frequency Control*, **56**(2), 314–325.

Juretzek, C. & Hadziioannou, C., 2016. Where do ocean microseisms come from? A study of Love-to-Rayleigh wave ratios, *Journal of Geophysical Research: Solid Earth*, **121**(9), 6741–6756.

Klinge, J., Schippkus, S., Walda, J., Hadziioannou, C., & Gajewski, D., 2025. Predictive modeling of seismic wave fields: learning the transfer function using encoder-decoder networks, *Geophysical Journal International*, p. ggaf004.

Landès, M., Hubans, F., Shapiro, N. M., Paul, A., & Campillo, M., 2010. Origin of deep ocean microseisms by using teleseismic body waves, *Journal of Geophysical Research: Solid Earth*, **115**(B5).

Li, S., Yang, C., Sun, H., & Zhang, H., 2019. Seismic fault detection using an encoder–decoder convolutional neural network with a small training set, *Journal of Geophysics and Engineering*, **16**(1), 175–189.

Li, W., Chakraborty, M., Fenner, D., Faber, J., Zhou, K., Rümpker, G., Stöcker, H., & Srivastava, N., 2022. EPick: Attention-based multi-scale UNet for earthquake detection and seismic phase picking, *Frontiers in Earth Science*, **10**.

Longuet-Higgins, M. S. & Jeffreys, H., 1950. A theory of the origin of microseisms, *Philosophical Transactions of the Royal Society of London. Series A, Mathematical and Physical Sciences*, **243**(857), 1–35.

Lu, J. Y., Zou, H., & Greenleaf, J. F., 1994. Biomedical ultrasound beam forming., *Ultrasound in medicine &*

biology, **20**(5), 403–428.

Lu, Y., Pedersen, H. A., Stehly, L., & Group, A. W., 2022. Mapping the seismic noise field in europe: spatio-temporal variations in wavefield composition and noise source contributions, *Geophysical Journal International*, **228**(1), 171–192.

Luijten, B., Cohen, R., de Bruijn, F. J., Schmeitz, H. A. W., Mischi, M., Eldar, Y. C., & van Sloun, R. J. G., 2020. Adaptive Ultrasound Beamforming Using Deep Learning, *IEEE Transactions on Medical Imaging*, **39**(12), 3967–3978.

Mousavi, S. M., Ellsworth, W. L., Zhu, W., Chuang, L. Y., & Beroza, G. C., 2020. Earthquake transformer—an attentive deep-learning model for simultaneous earthquake detection and phase picking, *Nature Communications*, **11**(1), 3952.

Pedersen, H. & Colombi, A., 2018. Body waves from a single source area observed in noise correlations at arrival times of reflections from the 410 discontinuity, *Geophysical Journal International*, **214**(2), 1125–1135.

Rost, S. & Thomas, C., 2002. ARRAY SEISMOLOGY: METHODS AND APPLICATIONS, *Reviews of Geophysics*, **40**(3), 2–1–2–27.

Rost, S. & Thomas, C., 2009. Improving Seismic Resolution Through Array Processing Techniques, *Surveys in Geophysics*, **30**(4), 271–299.

Ruigrok, E., Gibbons, S., & Wapenaar, K., 2017. Cross-correlation beamforming, *Journal of Seismology*, **21**(3), 495–508.

Schweitzer, J., Fyen, J., Mykkeltveit, S., Gibbons, S. J., Pirli, M., Kühn, D., & Kværna, T., 2012. Seismic arrays, in *New manual of seismological observatory practice 2 (NMSOP-2)*, pp. 1–80, Deutsches GeoForschungsZentrum GFZ.

Tol, P., 2025. Paul tol's notes, colour schemes and templates.

van der Veen, A.-J., Leshem, A., & Boonstra, A.-J., 2004. Signal processing for radio astronomical arrays, in *Processing Workshop Proceedings, 2004 Sensor Array and Multichannel Signal*, pp. 1–10.

Wang, K., Lu, L., Maupin, V., Ding, Z., Zheng, C., & Zhong, S., 2020. Surface Wave Tomography of Northeastern Tibetan Plateau Using Beamforming of Seismic Noise at a Dense Array, *Journal of Geophysical Research: Solid Earth*, **125**(4), e2019JB018416.

Warnick, K. F., Maaskant, R., Ivashina, M. V., Davidson, D. B., & Jeffs, B. D., 2016. High-Sensitivity Phased Array Receivers for Radio Astronomy, *Proceedings of the IEEE*, **104**(3), 607–622.

Yin, J., Denolle, M. A., & He, B., 2022. A multitask encoder–decoder to separate earthquake and ambient noise signal in seismograms, *Geophysical Journal International*, **231**(3), 1806–1822.

Zhang, R., Boué, P., Campillo, M., & Ma, J., 2023. Quantifying P-wave secondary microseisms events: a comparison of observed and modelled backprojection, *Geophysical Journal International*, **234**(2), 933–947.

Zlydenko, O., Elidan, G., Hassidim, A., Kukliansky, D., Matias, Y., Meade, B., Molchanov, A., Nevo, S., & Bar-Sinai, Y., 2023. A neural encoder for earthquake rate forecasting, *Scientific Reports*, **13**(1), 12350.